Resources, Conservation & Recycling 192 (2023) 106937

Contents lists available at ScienceDirect

Resources, Conservation & Recycling

journal homepage: www.elsevier.com/locate/resconrec

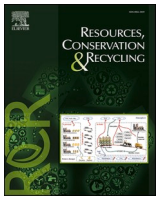

Full length article

Priority Lithium recovery from spent Li-ion batteries via carbothermal reduction with water leaching

Zhiming Yan *, Anwar Sattar, Zushu Li

WMG, University of Warwick, CV4 7AL, Coventry, United Kingdom

ARTICLE INFO

Keywords:
Spent Li-ion battery
Priority lithium recovery
Carbothermal reduction
Water leaching

ABSTRACT

Lithium is one of the most valuable elements within lithium-ion batteries, but it is also one of the least recycled metals owing to its high reactivity, solubility, and low abundance. This work presents an improved carbothermal reduction combined with a water leaching process for lithium recovery from $Li(Ni_xMn_yCo_{1-x-y})O_2$ cathode materials. Based on the thermodynamic analysis of the carbothermal reduction, the reduction products at different temperatures are clarified. The effects of various factors such as roasting temperature, liquid-solid ratio, and leaching time are assessed on lithium leaching efficiency. The reduced products are characterized by XRD, SEM-EDS, and SIMS. Results show that Co and Ni are reduced to metal, Mn remains as an oxide, whilst Li is converted mainly into Li_2CO_3 at temperatures lower than 800 ℃ and Li_2O when the temperature exceeds 900 ℃. Water leaching was used to efficiently extract lithium using low liquid-solid ratios. This improved lithium extraction process can effectively recover more than 93% of lithium as lithium hydroxide or carbonate at a purity greater than 99.5%. The effect of aluminium and copper impurities on the lithium recovery rate was investigated and it was found that copper has no significant effect on the lithium recovery rate, but the presence of aluminium decreases the lithium recovery rate through the production of lithium aluminate.

1. Introduction

A rapid increase in the production of lithium-ion batteries (LIBs) for electric vehicles (EVs) over recent years has sparked significant research into the appropriate treatment and recycling of spent LIBs. Furthermore, the target of achieving an 80% reduction in CO_2 emissions by 2050 has accelerated the development and deployment of hybrid electric vehicles (HEV), plug-in hybrid electric vehicles (PHEV) and battery electric vehicles (BEV). According to statistics, a typical BEV battery pack can weigh anywhere from 300 to 900 kg, and the lifetime of LIBs in EVs is currently between 8 and 10 years (Zheng et al., 2018). Most electrified vehicles utilise lithium-ion battery owing to its high power and energy densities as well as and long life. In 2021, 6.75 million EVs were sold worldwide with over 100% growth rate even during the pandemic, and BEVs stood for 71% of total sales (Paoli and Gul 2022). It is foreseeable that a large flow of LIBs at end-of-life (EoL) will require recycling in the near future. An EoL LIB is considered a hazardous waste but contains valuable resources that can be recycled (Latini et al., 2022).

Currently, there are three main EoL LIBs recycling routes, that is, high temperature processing via pyrometallurgy, leaching process via hydrometallurgy, and direct recycling without destruction of the crystalline structure. The pre-treatment is common to all the routes, including deactivation steps for lowing the electric and fire risks, and separation steps for separating active materials in black mass from other outputs (Hanisch et al., 2015; Zhang et al., 2018a). The cathode active material is the most valuable component in the LIB packages (Wentker et al., 2019), and $Li(Ni_xMn_yCo_{1-x-y})O_2$ attracts significant attention from recyclers due to its high content of valuable metals, especially the nickel, cobalt and lithium. Many methods have been proposed to recover these metals from the spent LIBs, which are well documented in the literature (Arshad et al., 2020; Liu et al., 2019a; Thompson et al., 2020; Makuza et al., 2021; Meng et al., 2021; Mansur et al., 2022).

High temperature processes can serve useful purposes with different temperature in certain circumstances, for example, thermal pre-treatment, extractive roasting, and smelting. Thermal pre-treatment processes operate at relatively low temperature (less than 600 ℃) and can be used to deactivate battery cells and even modules by safely decomposing the flammable organic carbonates, allowing the cells and modules to be processed without discharge (Chen et al., 2019; Yun et al., 2018; Kwade and Diekmann 2018). An added benefit of thermal

* Corresponding author.
E-mail address: Zhiming.yan@warwick.ac.uk (Z. Yan).

https://doi.org/10.1016/j.resconrec.2023.106937
Received 3 November 2022; Received in revised form 15 February 2023; Accepted 18 February 2023
Available online 22 February 2023

pre-treatment is that it enables easy separation of a high-quality black mass since the high temperatures also destroy the PVDF binder, enabling easy exfoliation of the powders from the foils. Smelting processes like Umicor (Umicore Group, 2019), use high temperatures over 1400 ℃ and carbon to reduce the metal oxides into liquid metals. The metals are then treated in a hydrometallurgical process where the valuable metals are recovered. Smelting processing is geared towards recovering the non-reactive metals such as nickel, cobalt, copper, and iron. Other components (both metal and non-metal) end up in the waste product, known as slag. Unfortunately, lithium is one of the metals that end up in the slag, along with aluminium and manganese, making them difficult to recover and recycle. Smelting processing is also not suitable for recycling Mn spinel oxides or $LiFePO_4$ cells (Makuza et al., 2021; Träger et al., 2015; Ren et al., 2017) as the carbon is not reactive enough to reduce phosphorus or the Mn. Extractive roasting provides a simple, versatile, and cost-effective method to treat spent LIBs, including salt-assisted and carbothermal reduction roasting. The principle of salt-assisted roasting is to convert the metal elements into water-soluble products that increase the leaching efficiency and reduce acid consumption. According to the reagent used, chlorination, sulfation, and nitration roasting are proposed (Fan et al., 2019; Lin et al., 2019; Shi et al., 2019; Lin et al., 2020; Peng et al., 2019). Since the metal salts are soluble in water, lithium still exists in the raffinate after the effective extraction of Co, Ni and Mn and faces the same problem of low lithium recovery rate. In the carbothermal reduction roasting processes, the cathode materials are reacted with a reducing agent such as graphite, coke, or dosage, leaving a mixture of metal/alloy intermediate compounds and excess carbon for further refining. In these processes, (Li et al., 2016; Mao et al., 2018; Tang et al., 2019; Xiao et al., 2017; Liu et al., 2019b), the reduction temperature is lower than 1000 ℃, the lithium forms Li_2CO_3 which can be leached out with water, and the metal oxides are reduced to a low valence state which is beneficial for acid leaching. However, a large amount of water is used during the water leaching due to the low solubility of Li_2CO_3 in water (1.3 g/100 g at 25 ℃ (Haynes 2014), resulting in the low concentration of lithium in leachate and more significant energy consumption during evaporation. Hu et al. (2017) proposed a carbonated water leaching can significantly decrease water consumption, but the lithium leaching efficiency is less than 85% and there is the problem of small amount of cobalt and nickel also leaching into the carbonated water. Li_2CO_3 is unstable at high temperatures, and the reducing gas is mainly CO formed from the Boudouard reaction ($C+CO_2=2CO$) which further promotes the decomposition of Li_2CO_3. Therefore, higher temperature carbothermic reduction is expected to yield Li_2O, which will be more beneficial for leaching and reducing water consumption.

The core of hydrometallurgy is leaching. Organic acids, inorganic acids as well as alkaline solution can be used for leaching while reducing agents are needed in some cases to enhance the leaching process. Pure metal salts are obtained after purification and solvent extraction, but lithium recovery is difficult and uneconomical from the raffinate with very low lithium concentration and high impurities from incomplete separation (Dhiman and Gupta 2019; Liu et al., 2019a; Wesselborg et al., 2021). Functionalized materials have unexpected effects on impurities removal and element capture (Shahat et al., 2018; Awual et al., 2019). In the battery recycling process, the Cu removal, Co(ii) /Ni(ii) capture and enrichment are challenging, and these functional materials will be a potentially powerful tool. The direct recycling route shows great potential in cost and environment, especially for NMC and NCA with high-value metals (Ciez and Whitacre, 2019; Sloop et al., 2018; Sloop et al., 2020). However, it is hard to scale up due to technical difficulties, such as the ideal separation of cathode materials from black mass and the specificity process of one-chemistry.

In this work, a process is developed to recover the lithium from black mass, prior to the acid leaching, at high efficiency and high purity. This paper focuses on the carbothermic reduction at higher temperature to form Li_2O and the following water leaching of lithium recovery from Li$(Ni_xMn_yCo_{1-x-y})O_2$. Various operating parameters were studied and optimized. Furthermore, the effects of the impurities (Al and Cu) on the efficiency and purity of lithium recovery were investigated. In this proposed process, graphite is utilized in situ, lithium can be extracted with a small amount of water, and no reductant is required in the acid leaching process, which are all beneficial in reducing energy consumption and cost. This process shows high practicability and wide application prospect.

2. Material and methods

The reagents and equipment used in this work are listed in Table 1. High purity, battery grade Li$(Ni_xMn_yCo_{1-x-y})O_2$ (LCO: $x = 0, y = 0$; NMC111:$x = 1/3, y = 1/3$; NMC622: $x = 0.6$, $y = 0.2$; NMC811: $x = 0.8$, $y = 0.1$), Li_2CO_3, graphite, Al and Cu foil were used in current work for the following experiments. All the samples with the desired composition were mixed well using Thinky ARE-250 at 1000 rpm for 5 min.

2.1. TGA/DSC+QMS analyses

The thermogravimetric analyzer and differential scanning calorimetry (TGA-DSC) coupled with quadrupole mass spectrometer (QMS) was used to study the carbothermal reduction of Li$(Ni_xMn_yCo_{1-x-y})O_2$. The mixed sample was heated in the TGA furnace from room temperature to 1100 ℃ with a heating rate of 10 ℃/min in a 50 ml/min argon atmosphere. The off-gas composition was analyzed by the QMS to confirm the reduction of gas products. TGA was used to investigate the decomposition of raw Li$(Ni_xMn_yCo_{1-x-y})O_2$ powder and Li_2CO_3. Thermodynamic calculations were performed using HSC Chemistry 10 (http://www.hsc-chemistry.net) and FactSage 8.1 (https://www.factsage.com) to obtain the corresponding Gibbs free energies for the reactions.

2.2. Reduction roasting

The carbothermal reduction experiments were conducted in a tube furnace. The well-mixed sample (20 g) was roasted at the target temperature for 1 h with a heating rate of 10 ℃/min in a 300 ml/min argon flow. The effect of reduction temperature (700–1200 ℃) on the lithium recovery was studied using NMC111 to optimize the reduction temperature. The effect of impurities (Al foil and Cu foil) on lithium recovery in the optimized process were investigated. A graphite crucible

Table 1
Reagents and equipment used in the experiments.

Reagents	Purity	Company	Country
Li$(Ni_xMn_yCo_{1-x-y})O_2$	99.80% (battery grade)	TARGRAY	Canada
Li_2CO_3	99.00% (ACS reagent)	Sigma-Aldrich	USA
Graphite	99.99% (battery grade)	Merck Life Science Ltd.	UK
Al foil/Cu foil	99.95% (battery grade)	Thermo Scientific	UK
Equipment	**Model**	**Company**	**Country**
Mixer	Thinky ARE-250	THINKY	Japan
TGA-DSC	STA 449 F3 Jupiter	NETZSCH	Germany
QMS	HPR20	HIDEN Analytical	UK
Tube furnace	HZS 1200℃	Carbolite Gero Ltd.	UK
Vibrating disc miller	Scheibenschwing-TS 750	SIEBTECHNIK TEMA	Netherlands
PSD analyzer	Mastersizer range 3000	Malvern Panalytical	UK
Ultrasonic Bath	Elmasonic S 30 H	ELMA	Germany
Centrifuge	Micro 17	ThermoFisher	UK
ICP-OES	5110 ICP-OES	Agilent Technologies	USA
XRD	Aeris	Malvern Panalytical	UK
SEM/EDS+SIMS	Dual-beam SEM system	FEI	USA

was used since the lithium oxides will react with corundum/quartz crucible at high temperature, affecting the recovery of lithium. After roasting, the samples were weighted to obtain mass loss and then crushed by a vibrating disc mill machine. The particle size distribution (PSD) of the powders before and after reduction were analyzed using Mastersizer range 3000. The samples before and after roasting were detected by X-ray diffraction (XRD), equipped with Cu K α radiation: 1.5406 Å, scanning rate: 0.0236°/s, ranges: 5–90°. The morphology and components of the samples were analyzed with scanning electron microscopy and energy-dispersive X-ray spectroscopy (SEM-EDS). In contrast, the lithium distribution of the reduced sample was detected by secondary ion mass spectrometry (SIMS).

2.3. Selective leaching

Water leaching of the reduced sample powder was carried out in a 50 ml flask with an ultrasonic bath since the magnet will attract the cobalt/nickel alloy in the reduced products. Effects of liquid/solid ratio (3 – 10 ml/g) and leaching time on the lithium leaching efficiency were investigated. Roasted powder and deionized water were added to the reactor

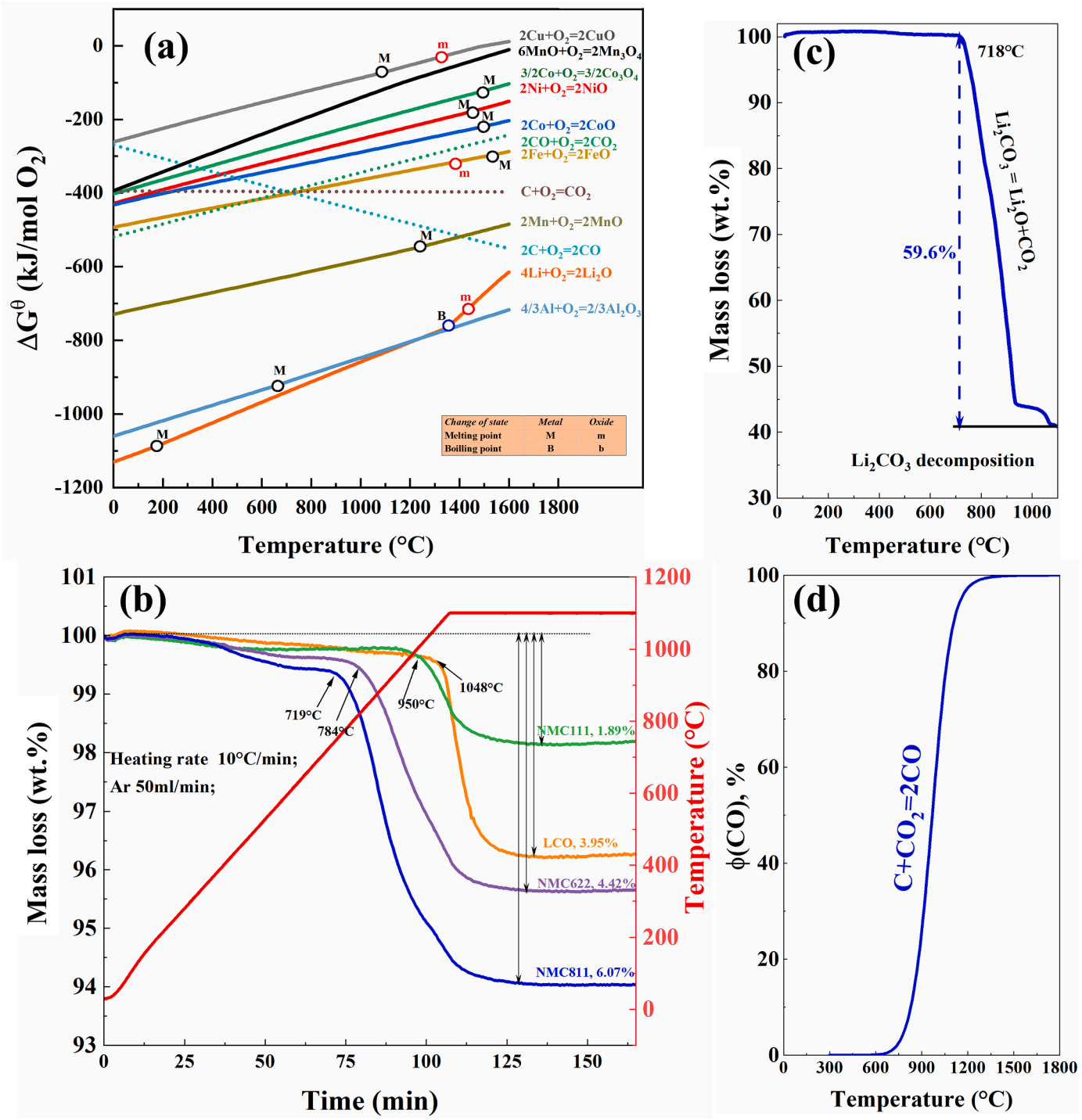

Fig. 1. (a) Ellingham diagram for several metals in Li-batteries, (b) TGA-DSC result for pyrolysis of $Li(Ni_xMn_yCo_{1-x-y})O_2$ in argon, (c) TGA result for decomposition of Li_2CO_3 in argon, and (d) equilibrium diagram of CO partial pressure for the Boudouard reaction.

at a designed liquid/solid ratio. After a predetermined leach time, the solution was filtered by syringe filtration, and the metal contents in the leachate were analyzed by ICP-OES. The optimal roasting temperature and liquid-solid ratio were determined using the leaching efficiency of the lithium. After roasting and leaching under optimized conditions, CO_2 gas was injected into the solution to convert the LiOH into Li_2CO_3 which was then recovered and dried. The lithium-less residue was subjected to acid leaching to determine the remaining Co, Mn, Ni, and carbon. All the acid leaching tests were conducted using 2 mol/L HNO_3 in a 50 ml flask with a liquid-solid ratio of 20 ml/g in an ultrasonic bath at room temperature for 2 h. The Co, Mn, and Ni contents were analyzed using ICP-OES and the remaining graphite was recovered, dried, and weighed. The powder before and after water leaching and the obtained lithium carbonate were characterized by XRD.

The leaching efficiency η of element i is calculated as:

$$\eta_i = \frac{c_i V}{m_0 w_i} \times 100\%$$

where m_0 is the mass of the raw material, g; w_i is the mass percentage of element i in raw material. c_i is the concentration of element i in the leachate, g/mL; and the V is the volume of leachate, ml.

3. Results and discussion

3.1. Thermodynamic study

The Mn valence state in $Li(Ni_xMn_yCo_{1-x-y})O_2$ is exclusively Mn^{4+}, and the occupation of Ni^{3+} steadily increases at the cost of Ni^{2+} with increasing Ni content. The fraction of Co^{3+} first decreases and then gradually increases when the Ni composition increases. (Sun and Zhao 2017). The $Li(Ni_xMn_yCo_{1-x-y})O_2$ can be decomposed at high temperatures into Li_2O, CoO, NiO, Mn_3O_4 and O_2 since these oxides are more stable at high temperatures (Haynes 2014), and the possible reaction is

$$LiNi_xMn_yCo_{1-x-y}O_2 = \frac{1}{2}Li_2O + xNiO + (1-x-y)CoO + \frac{y}{3}Mn_3O_4 + \left(\frac{3-2y}{12}\right)O_2(g) \quad (1)$$

An Ellingham diagram is used to present the equilibrium temperature between an element, its oxide, and oxygen, which can be used to determine whether an oxide will be reduced. According to Fig. 1(a), the oxides of Co, Ni, Fe, and Cu can be reduced to the metal phase by solid carbon or carbon monoxide above 800 ℃. The stable phase of manganese oxides under reducing conditions below 1400 ℃ is MnO. Li_2O and Al_2O_3 are very stable that cannot be reduced by carbon. Therefore, after carbothermic reduction of $Li(Ni_xMn_yCo_{1-x-y})O_2$, cobalt and nickel exist in metallic form, while manganese and lithium exist in oxide form and the Mn valence state is Mn^{2+}. From Fig. 1(b), the temperature at which LCO decomposes is about 1048 ℃. For NMC, the decomposition temperature decreases from 950 ℃ to 719 ℃ with increasing Ni content. The mass loss of LCO is about 3.7%, but the mass loss of NMC increases with increasing Ni content indicating that the Ni reduces the stability of NMC at high temperatures. The mass loss of these samples is less than the theoretical mass loss of reaction (1), indicating that although Li $(Ni_xMn_yCo_{1-x-y})O_2$ is unstable at high temperatures, its decomposition is incomplete. When graphite is present, the activity of oxides and oxygen partial pressure in reaction (1) will be decreased due to redox, resulting in a decrease in the theoretical decomposition temperature. The redox products are Co, Ni, MnO, CO or CO_2. The Li_2O will react with CO_2:

$$Li_2O + CO_2(g) = Li_2CO_3, \Delta G_r^\theta = -210.47 + 0.1349T, kJ(0 \sim 1800^\circ C) \quad (2)$$

However, the Li_2CO_3 (melting temperature is 723 ℃ (Haynes 2014) will decompose quickly after melting and releasing CO_2. It is almost completely decomposed at 1000 °C (The theoretical mass loss for complete decomposition is 59.55%), as shown in Fig. 1(C). In carbothermic reduction, the gasification reaction of carbon (also called the Boudouard reaction, Eq.(3)) has a significant effect on the reduction that cannot be ignored. Due to the limitation of solid-phase diffusion, the solid-solid reaction rate is prolonged, and the CO generated by the gasification reaction will become the primary reducing agent for reducing the oxides. As shown in Fig. 1(d), the CO_2 can be reduced by C to CO when the temperature is above 702 ℃, and the partial equilibrium pressure of CO rises rapidly after 850 ℃. Hence, it can be seen that the initial CO_2, produced from the reduction of the metals, is itself reduced by the carbon via the Boudouard reaction to produce CO. Therefore, reaction Eq. (4) should be considered the main reaction at high temperatures:

$$C + CO_2 = 2CO, \Delta G_r^\theta = 170.20 - 0.174T\text{kJ}(0 \sim 1800^\circ C) \quad (3)$$

$$LiNi_xMn_yCo_{1-x-y}O_2 + \left(\frac{3}{2}-y\right)C = \frac{1}{2}Li_2O + (1-x-y)Co + xNi + yMnO + \left(\frac{3}{2}-y\right)CO(g) \quad (4)$$

The results of TGA-DSC coupling QMS for carbothermal reduction of LCO and NMC111 are shown in Fig. 2. The mass loss starts at around 790 ℃ and finish below 1000 ℃ and is less than the theoretical mass loss for the reaction (4) (theoretical mass loss for LCO is 35.15%, and for NMC111 is 28.54%). An obvious endothermic peak can be seen around 700 ℃ for the LCO, whilst it is weaker for NMC111; indicating that the metal oxide reduction reactions have begun, and the produced CO_2 is captured by Li_2O, to produce Li_2CO_3, resulting in no mass change. The distinct endothermic peaks over 800 ℃ are mainly attributed to the reduction and decomposition reactions. The QMS results show that the initial mass loss is due to the release of CO_2 and the CO content in off-gas increases rapidly when the temperature is above 900 ℃, which is further evidence that reaction (4) is the dominant reaction at high temperatures. The CO_2 in off-gas was detected when the temperature was over 780 ℃, which is higher than the pure Li_2CO_3 decomposition temperature (Fig. 1 (c)). The possible reason is that the partial pressure of CO_2 in the sample under reducing conditions is higher, which increases the decomposition temperature. The formation of CO_2 decreases carbon consumption, resulting in a lower mass loss of reaction (4) than the theoretical value. The results suggest that the possible reduction products of $Li(Ni_xMn_yCo_{1-x-y})O_2$ should be Li_2CO_3, Co-Ni alloy, MnO, and CO_2 at low temperatures (600–800 ℃). Due to the limitations of kinetic conditions at low temperatures, such as solid-phase diffusion, the reduction may not be complete, resulting in the existence of CoO and NiO. The Li_2O and CO will replace Li_2CO_3 and CO_2 as the main products at higher temperatures (over 900 ℃).

3.2. Carbothermal reduction

Based on the thermodynamic analysis and TGA-DSC-QMS results, the reduction of NMC111 was conducted from 800 ℃ to 1200 ℃ for 1 h in the Ar atmosphere with 20% excess graphite. An additional three hours of roasting at 1000℃ was conducted to investigate the effect of roasting time on lithium recovery. Fig. 3(a) shows the effect of reduction temperature on mass loss. There is about a 5% mass loss in the sample with the roasted temperature at 800 ℃, and the mass loss increased with increasing temperature. Increasing the roasting time from one hour to three hours at 1000 ℃ increases the mass loss, and the mass loss is higher than theoretical mass loss when the temperature is over 1000 ℃. The possible reason is that the phase containing lithium may be volatilized at high temperatures. (Hu et al., 2017) Therefore, the optimized conditions are that the reduction temperature should not be higher than 1000 ℃, and the reduction time should not exceed 1 h. The XRD detections of the samples after roasting are shown in Fig. 3(b). When the

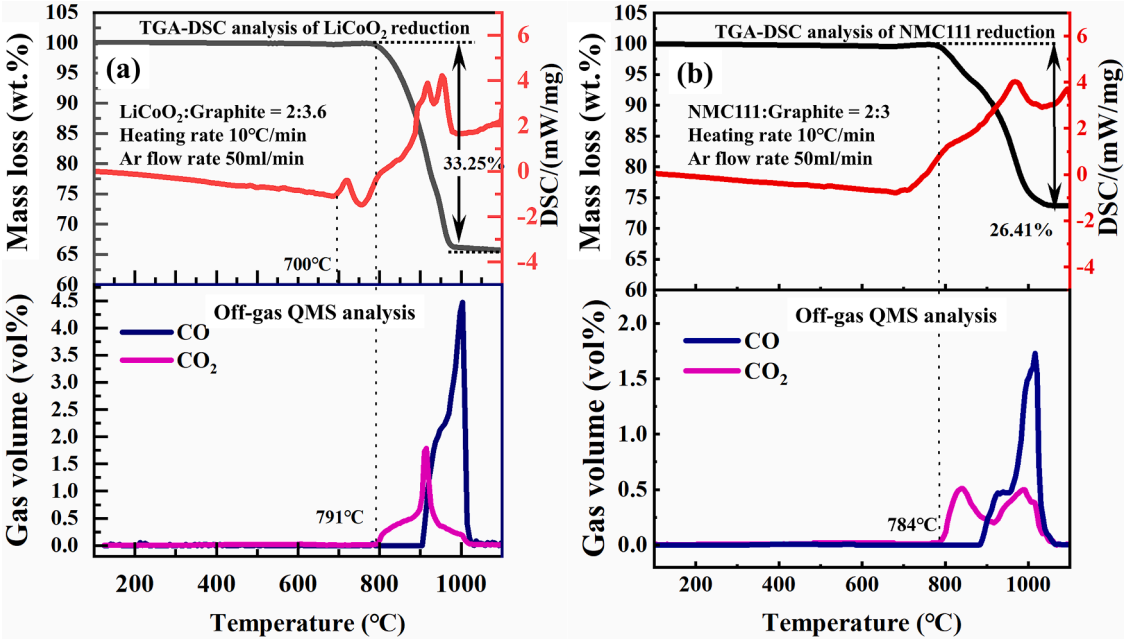

Fig. 2. The results of TGA-DSC coupling QMS for carbothermal reduction of LCO (a) and NMC111 (b).

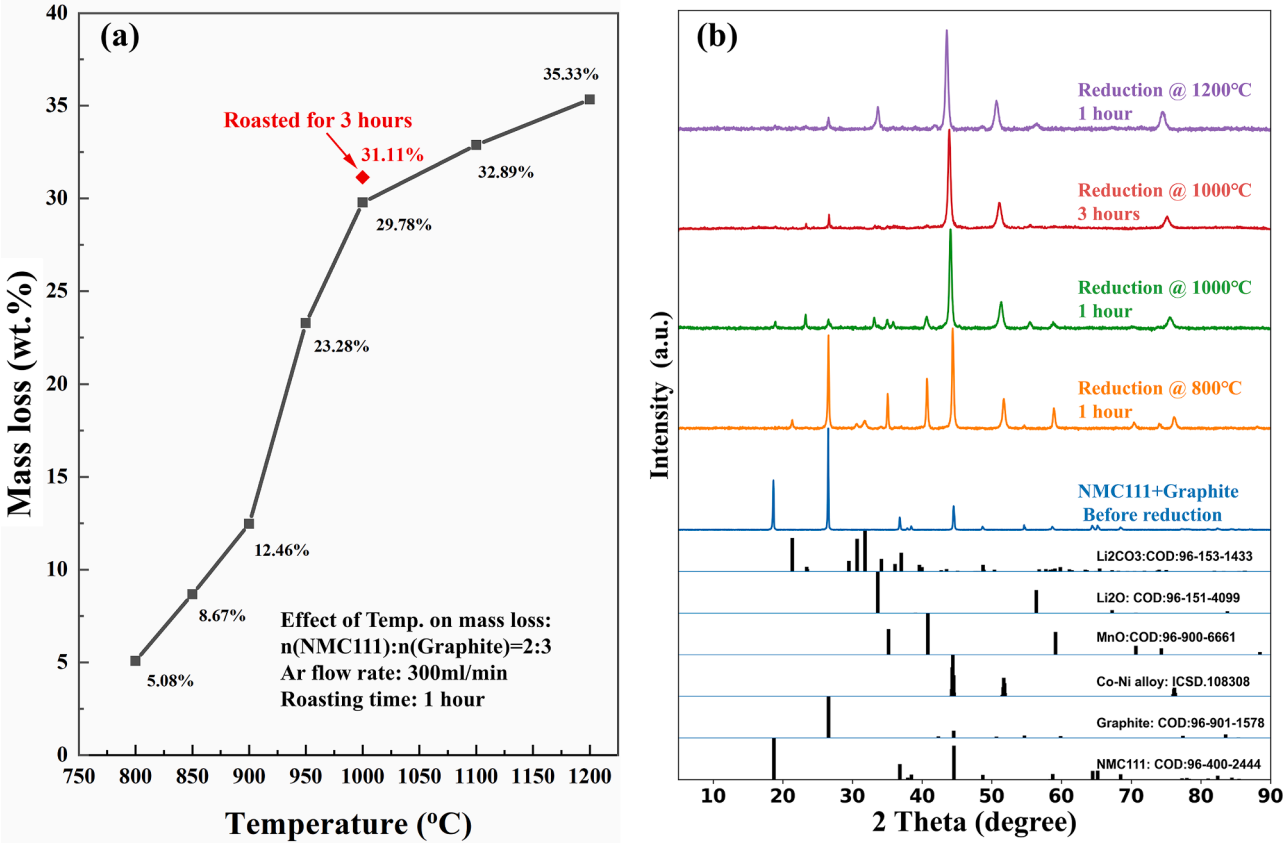

Fig. 3. Effect of roasting temperature on (a) the mass loss and (b) XRD patterns of the reduced samples.

temperature was set to 800 ℃, Li_2CO_3, Co-Ni alloy, graphite, and MnO were detected. The structure of NMC111 has been destroyed since no detectable peaks were found. With increasing temperature, the peak intensity of Co-Ni alloy and Li_2O improve significantly. The peaks of Li_2CO_3 are hard to spot after being roasted at 1000 ℃. An obvious peak around 23° in the reduced sample at 1000 ℃ cannot be identified by XRD and disappears after water leaching. It may be a lithium-manganese compound, which can react with or dissolve into the water but not affect the recovery of lithium. As the graphite is consumed, the peak intensity decreases, but it is still evident due to the excess amount. It should be noted that since MnO changes its structure under high temperature reduction conditions, the peak of MnO almost disappears after roasting

at 1000 ℃ for three hours or 1 h at 1200 ℃. The above results confirm that lithium exists in the form of oxides in the samples after high temperature reduction.

The morphology and particle size distribution of NMC111 with graphite mixture before and after reduction are shown in Fig. 4(a-b). Before reduction, the particle size of the sample is concentrated between 9 and 34 um (D_v(10)-D_v(90)), and the surface of the sample is relatively smooth. While for the reduced sample after crushing, the particle size distribution range becomes wider (D_v(10)-D_v(90): 1.8–51 um) with rougher surfaces. The increase in particle size is mainly due to the aggregation and growth of Co-Ni alloy. The solid phase growth benefits from its contact; increasing the graphite content reduces the chance of metallic contact, which is favourable for crushing. The higher graphite content does not affect the quality of lithium recovery. Since oxides are brittle compared to metal, Li_2O and MnO are easier to break and form fine particles. Fig. 4(c–h) presents the cross-section of a typical particle of the reduced sample and the distribution of the elements. The whole particle is formed by the aggregation of metals and oxides, and part of MnO is tightly stuck with Co-Ni alloy. Although Co-Ni alloy is magnetic, oxides stick to Co-Ni alloy in the products, making magnetic separation impossible to separate Co-Ni and oxides effectively. Fig. 4(i) shows a schematic diagram of the reduction and crushing processes. During the

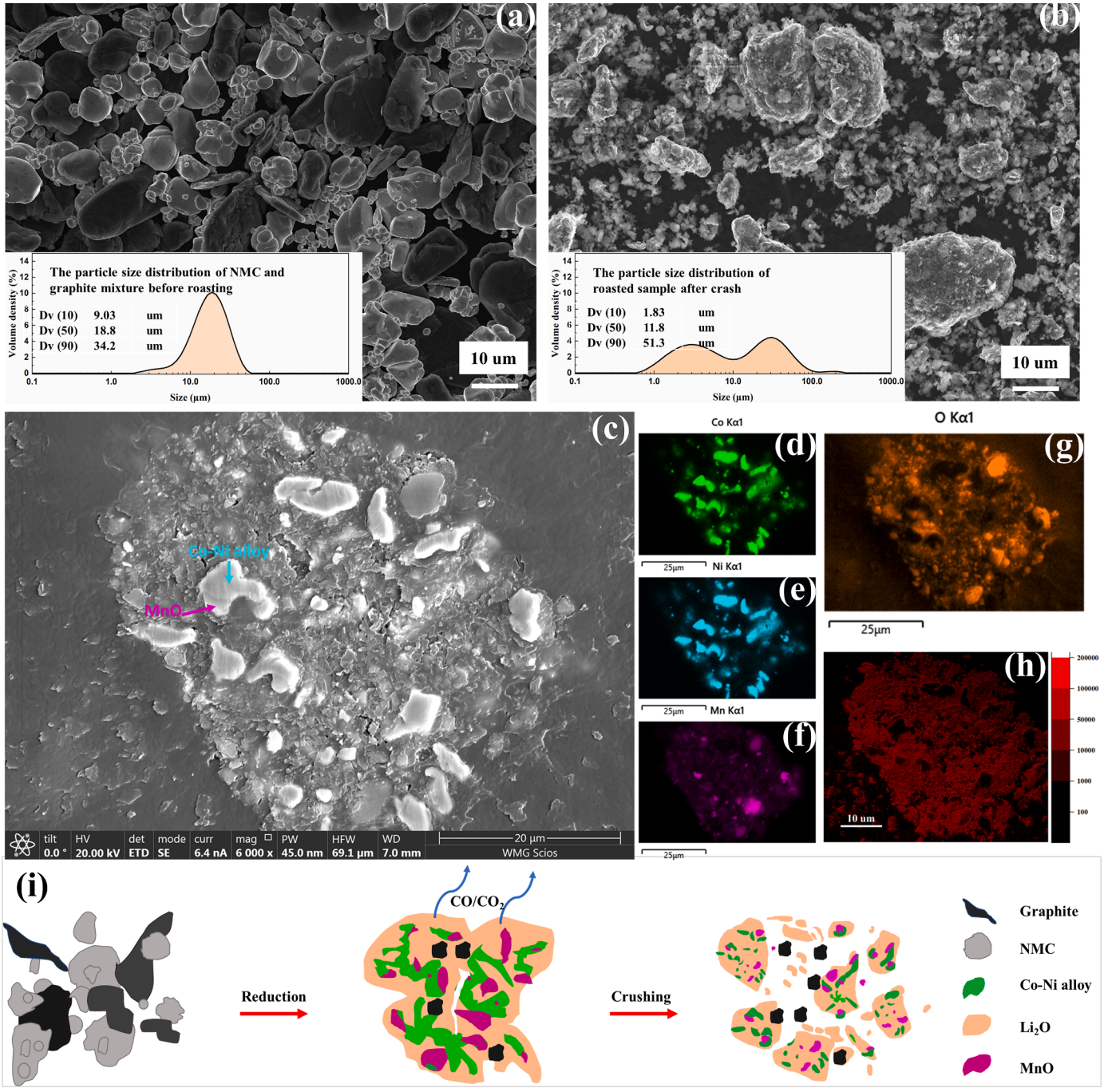

Fig. 4. (a) Morphology and particle size distribution of NMC111 and C mixture before reduction roasting; (b) Morphology and particle size distribution of reduced sample at 1000 ℃ after crushing; (c) Cross-sectional morphology of the reduced sample 1000℃ (after crushing); (d) EDS analysis – distribution of Co; © EDS Analys– – distribution of Ni; (f) EDS Analys– – distribution of Mn; (g) EDS Analys– – distribution of O; (h) ToF-SIMS Analys– – distribution of Li; (i) Schematic diagram of reduction and crushing processes.

reduction process, the graphite is consumed and generates CO/CO_2 leaving the system, and the Co-Ni alloy nucleates and grows. The oxides sinter and adhere to the Co-Ni alloy interstices, preventing the further growth of metallic to a certain extent. Due to the release of gas, the product is not particularly dense, which facilitates crushing. In the crushing process, the oxides (as well as the remaining graphite) are crushed into fine particles due to the difference in strength compared with the metallic alloy. Other parts of the oxides will adhere to the depressions on the surface of the alloy particles due to the protection of the metal.

3.3. Selective leaching

After the high temperature carbothermic reduction and crushing, the solid products are still mixed and mainly include Li_2O, MnO, Co-Ni alloy, and unreacted graphite (C). When the carbothermic reduction occurs at a lower temperature, lithium mainly exists in Li_2CO_3. Although water leaching is also possible, it consumes a lot of water and requires a lot of energy to evaporate. Considering that Li_2O can react with water and release lots of heat (Eq. (5)), its product LiOH is very soluble in water (12.5 g/100 g H_2O at 25℃) (Haynes 2014), water leaching could be an efficient way to separate lithium from other substances. Li_2O solubility increases with temperature so the heat from the reaction also allows more lithium to leach into the water, thus increasing leaching efficiency. A small amount of water can leach out all the lithium, which significantly reduces the water consumption and the energy consumed to obtain Lithium products by evaporation.

$$1/2Li_2O + 1/2H_2O = LiOH, \Delta_f H_m^0 = -(487.46 \pm 0.1)\,\text{kJ}\ (25^\circ C) \quad (5)$$

The effects of reduction temperature, liquid-solid ratio, and leaching time on the lithium leaching efficiency were investigated, and the results are shown in Fig. 5(a–c). When the temperature is lower than 900 ℃, the lithium leaching efficiency is less than 50% and increases to 93.28% when the temperature is 1000 ℃. At low temperatures, most of the lithium in the sample was transformed into Li_2CO_3, which cannot be leached out properly via water. With increasing temperature, Li_2CO_3 decomposed to Li_2O, increasing the lithium leaching efficiency. With increasing residence time and roasting temperature, the lithium leaching efficiency decreases mainly due to the lithium loss during the roasting process. Amass balance calculation shows that the minimum liquid-solid ratio required is less than 3 ml/g, and the lithium leaching efficiency obtained is about 90%. Increasing the liquid-solid ratio from 5 ml/g to 10 ml/g increases the lithium leaching efficiency slightly. This suggests that water leaching can extract lithium effectively at a low liquid-solid ratio. Due to the fast reaction rate of Li_2O with water, the leaching process can be completed quickly under favourable kinetic

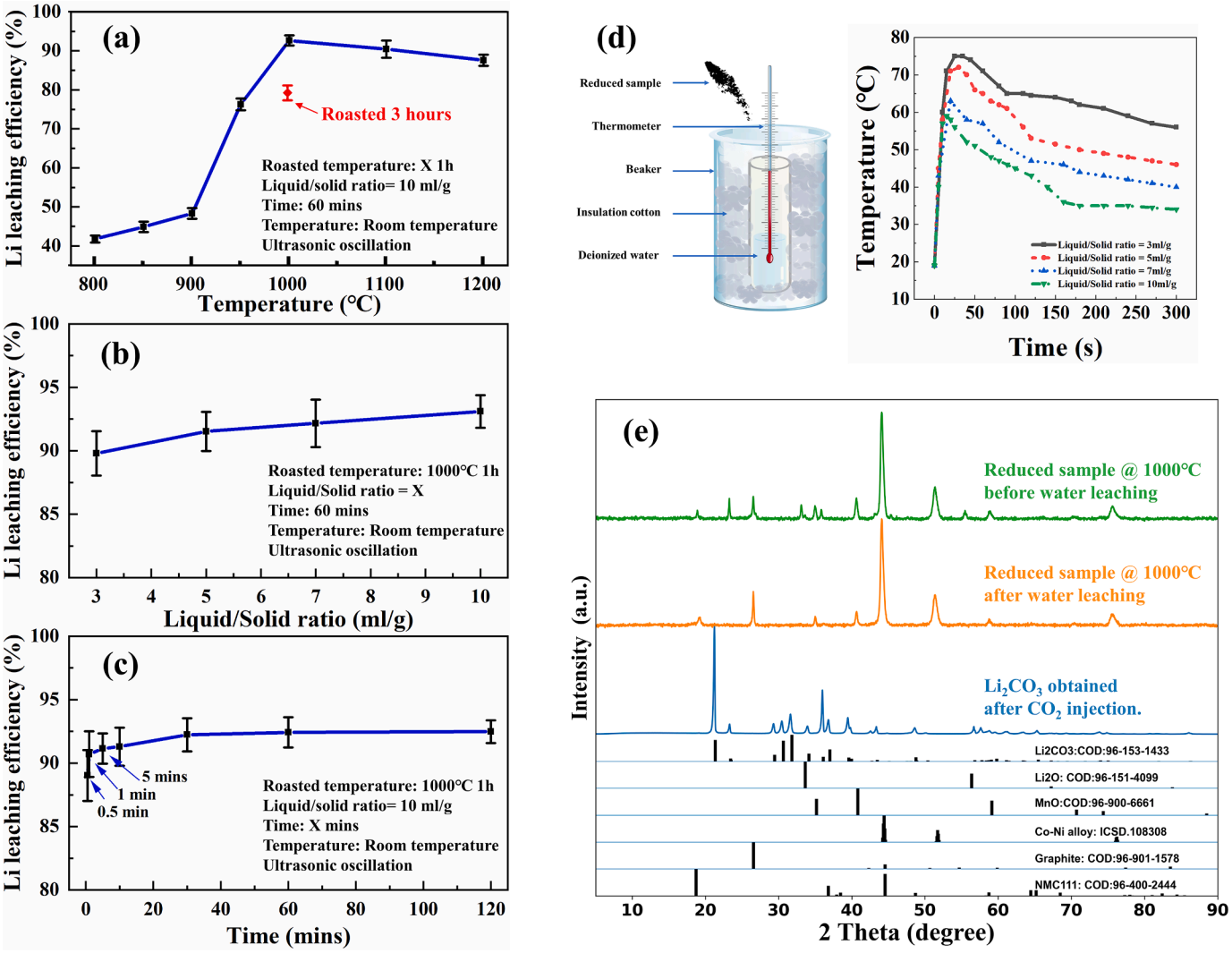

Fig. 5. (a) Effect of roasted temperature on the lithium leaching efficiency; (b) Effect of liquid-solid ratio on the lithium leaching efficiency; (c) Effect of water leaching time on the lithium leaching efficiency; (d) Schematic diagram of temperature measurement and the temperature changes with different liquid-solid ratios during water leaching; (f) XRD patterns of the reduced NMC111 sample before and after water leaching, and the obtained product after CO_2 injection.

conditions. The lithium leaching efficiency reached over 85% in 30 s, and no significant change after 30 mins. Fig. 5(d) presents the temperature changes with different liquid-solid ratios during water leaching, which clearly shows that a large amount of heat is released in the initial 50 s, and the temperature increases rapidly. Then the temperature gradually decreases and tends to be stabilise. The XRD patterns of the reduced sample before and after water leaching and evaporated product of the leachate after CO_2 injection are shown in Fig. 5(e). It is obvious that there are no Li_2O peaks found in the residue after water leaching. The leachate is aqueous LiOH, where the other metal elements from LIBs, such as Fe, Cu, Co, Ni, and Mn, have an extremely low solubility in this strong alkali solution (Zhang et al., 2018b). In this case, high purity LiOH is guaranteed from the water leaching process. LiOH can absorb CO_2 if it is dried directly in the air, resulting in a mixture of LiOH and Li_2CO_3. To obtain pure LiOH, a CO_2-free environment is required during the leaching and evaporation process. In addition, LiOH is known to be hygroscopic and can deliquescence, requiring controlled handling and storage facilities. Thus, CO_2 was injected into the leachate to convert LiOH to $LiHCO_3$, and then Li_2CO_3 product was obtained after evaporation. XRD and ICP-OES show that a high quality Li_2CO_3 was produced which had a purity of 99.5%. The preferable reduction temperature and roasting time were 1000 ℃ and 1 h, and the liquid-solid ratio and leaching time for the lithium effective extraction during water leaching was optimized at 5 ml/g and 30 min, respectively.

The solid residue remaining after water leaching was subjected to acid leaching to determine the Co, Ni, Mn contents and separate out the graphite. Since it has already been reduced, reducing agents such as H_2O_2 and $Na_2S_2O_3$ were not required. The ICP detection of the acid leachate shows that 96.96% of cobalt, 97.67% of nickel, and 99.22% of manganese were leached from the residue. According to the procedure described in publications (Devi et al., 1998, 2000), Co, Ni, and Mn can be extracted efficiently by solvent extraction methods.

3.4. Effect of impurities on lithium recovery

In the most common design of lithium batteries, the graphite layer is stuck onto a copper current collector, and the cathode metal oxide is stuck onto an aluminium current collector. After crushing, sieving, and separation, most of the aluminium and copper can be removed effectively, but there may still be a small amount of aluminium/copper impurities in the black mass. It is easy to obtain the black mass with the content of aluminium and copper foil in less than 2%, but further purification costs skyrocket. Therefore, it is vital to investigate the effects of aluminium and copper impurities on the efficiency of lithium recovery.

Fig. 6(a, b) show the effect of aluminium and copper on the mass loss and lithium leaching efficiency of LCO and NMC111 during the reduction and water leaching processes. The copper impurity shows no significant effect on mass loss and lithium leaching efficiency. In contrast, increasing aluminium content decreases the mass loss and lithium leaching efficiency. According to the Ellingham diagram (Fig. 1(a)), copper exists in the form of metal during the reduction roasting process and will not react with lithium oxide. While aluminium is very reactive and easily captures oxygen as a reductant to form alumina, resulting in less oxygen releases and reduces the mass loss. The alumina reacts with lithium oxide to form lithium aluminates (Eq.6). The Li leaching efficiency is not changed when the aluminium content is less than 1.0 wt.% and decreases with further increases in aluminium content meaning that the formed lithium aluminate has a certain solubility in a strong alkali solution. When the aluminium content in the black mass is less than 1.0 wt.%, the generated lithium aluminate will dissolve, which will not affect the lithium leaching efficiency. When the aluminium content in the black mass is higher than 1 wt.%, the lithium aluminate will not be completely dissolved, and the lithium leaching efficiency decreases. Fig. 6(c) shows the XRD patterns of the reduced LCO with copper and aluminium addition. Distinct XRD peaks of metallic copper in the reduced sample with copper addition, while the Li_5AlO_4 is formed in the reduced sample with aluminium impurity, which can be evidenced from the XRD patterns of the LCO reduced sample. Since the aluminium deteriorates the lithium recovery, the carbothermal reduction with water leaching process requires low aluminium content in the raw material.

$$5Li_2O + Al_2O_3 = 2Li_5AlO_4, \Delta G_r^{\theta} = -93.44 - 0.0204T\,\mathrm{kJ}(0 \sim 1500^{\circ}C) \quad (6)$$

Through the carbothermal reduction combined selective leaching process, the $Li(Ni_xMn_yCo_{1-x-y})O_2$ cathode materials of end-of-life LIBs is recycled into the products of Li_2CO_3, carbon, and Co/Ni/Mn salts, all of

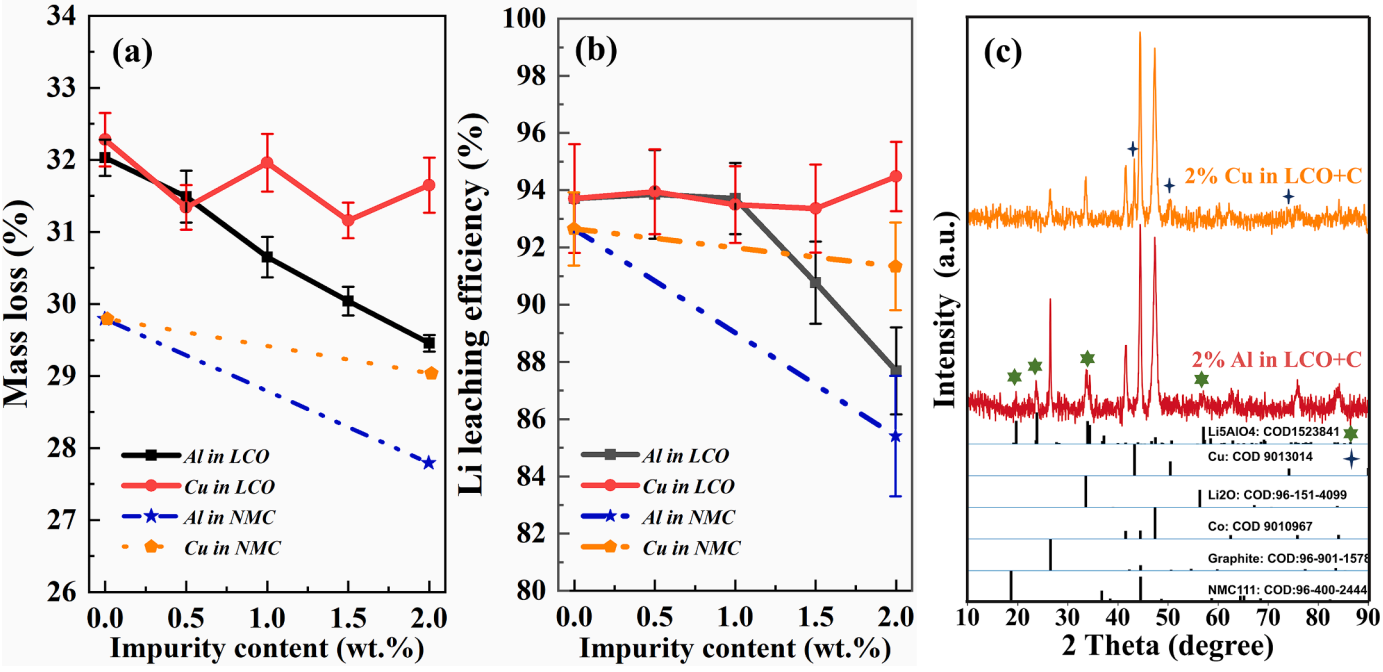

Fig. 6. Effect of copper and aluminium on the reduction of mass loss (a) and lithium leaching efficiency (b) of LCO and NMC; (c) XRD patterns of the reduced LCO samples with 2% of copper and aluminium impurities.

which are valuable materials. In this process, the part of anode graphite is utilized in situ to act as a reductant, lithium can be preferentially extracted after reduction by a small amount of water, and no reductant is needed in the acid leaching process. These are all beneficial in reducing the energy consumption and cost of the recycling process. This process shows high practicability and broad application prospect.

4. Conclusions

The priority lithium recovery from EoL LIBs strategy was successfully demonstrated via an improved carbothermal reduction combined water leaching process. According to the thermodynamic analysis and roasting experiments, after carbothermal reduction, the Co and Ni are reduced to metal, while Mn in the form of MnO. Lithium is mainly in Li_2CO_3 when temperature is lower than 800℃ but primarily transformed into Li_2O when temperature over 900 ℃. After roasting at 1000 ℃ for 1 h, almost all the lithium exists in the form of Li2O in the reduction product, then the lithium can be preferentially extracted efficiently by water leaching with a low liquid-solid ratio (5 ml/g) in 30 min. Since the strong alkalinity of the leachate, high purity Li_2CO_3 (>99.5%) can be guaranteed by evaporating the carbonated solution. The copper impurity shows no significant effect on lithium recovery rate, while aluminium decreases the lithium recovery rate because the formed lithium aluminate has low solubility in leachate. In the improved carbothermal reduction with water leaching process, graphite is utilized in situ, high-purity lithium product can be extracted efficiently and fast with a small amount of water, and no reductant in the acid leaching process, which are all beneficial in reducing energy consumption and cost. This process shows high practicability and wide application prospect.

CRediT authorship contribution statement

Zhiming Yan: Conceptualization, Methodology, Software, Data curation, Formal analysis, Writing – original draft. **Anwar Sattar:** Supervision, Writing – review & editing, Funding acquisition. **Zushu Li:** Supervision, Writing – review & editing, Project administration.

Declaration of Competing Interest

The authors declare that they have no known competing financial interests or personal relationships that could have appeared to influence the work reported in this paper.

Data availability

Data will be made available on request.

Acknowledgements

This work was carried out as part of the RECOVAS Project (75730) which was part funded by the Advanced Propulsion Centre. The authors thank Dr David Walker from the X-ray Diffraction Research Technology Platform at Warwick for running the XRD measurements.

References

Arshad, F., Li, L., Amin, K., Fan, E., Manurkar, N., Ahmad, A., Yang, J., Wu, F., Chen, R., 2020. A comprehensive review of the advancement in recycling the anode and electrolyte from spent lithium ion batteries. ACS Sustain. Chem. Eng. 8 (36), 13527–13554. https://doi.org/10.1021/acssuschemeng.0c04940.

Awual, M.R., Hasan, M.M., Rahman, M.M., Asiri, A.M., 2019. Novel composite material for selective copper (II) detection and removal from aqueous media. J. Mol. Liq. 283, 772–780. https://doi.org/10.1016/j.molliq.2019.03.141.

Chen, M., Ma, X., Chen, B., Arsenault, R., Karlson, P., Simon, N., Wang, Y., 2019. Recycling end-of-life electric vehicle lithium-ion batteries. Joule 3 (11), 2622–2646.

Ciez, R.E., Whitacre, J.F., 2019. Examining different recycling processes for lithium-ion batteries. Nat. Sustain. 2, 148–156. https://doi.org/10.1038/s41893-019-0222-5.

Devi, N.B., Nathsarma, K.C., Chakravortty, V., 1998. Separation and recovery of cobalt (II) and nickel(II) from sulphate solutions using sodium salts of D2EHPA, PC 88A and Cyanex 272. Hydrometallurgy 49 (1), 47–61. https://doi.org/10.1016/S0304-386X(97)00073-X.

Devi, N.B., Nathsarma, K.C., Chakravortty, V., 2000. Separation of divalent manganese and cobalt ions from sulphate solutions using sodium salts of D2EHPA, PC 88A and Cyanex 272. Hydrometallurgy 54 (2), 117–131. https://doi.org/10.1016/S0304-386X(99)00054-7.

Dhiman, S., Gupta, B., 2019. Partition studies on cobalt and recycling of valuable metals from waste Li-ion batteries via solvent extraction and chemical precipitation. J. Clean. Prod. 225, 820–832. https://doi.org/10.1016/j.jclepro.2019.04.004.

FactSage, 8.2.2022.. https://www.factsage.com.

Fan, E., Li, L., Lin, J., Wu, J., Yang, J., Wu, F., Chen, R., 2019. Low-temperature molten-salt-assisted recovery of valuable metals from spent lithium-ion batteries. ACS Sustain. Chem. Eng. 7 (19), 16144–16150.

Hanisch, C., Diekmann, J., Stieger, A., Haselrieder, W., Kwade, A., 2015. Recycling of lithium-ion batteries. Handb. Clean Energy Syst. 1–24. https://doi.org/10.1002/9781118991978.HCES221.

Haynes, W.M., 2014. CRC Handbook of Chemistry and Physics. CRC press.

Hu, J., Zhang, J., Li, H., Chen, Y., Wang, C., 2017. A promising approach for the recovery of high value-added metals from spent lithium-ion batteries. J. Power Sources 351, 192–199. https://doi.org/10.1016/j.jpowsour.2017.03.093.

Kwade, A., Diekmann, J., 2018. Recycling of Lithium-Ion Batteries. The LithoRec Way, Switzerland: Springler International Publishing AG.

Latini, D., Vaccari, M., Lagnoni, M., Orefice, M., Mathieux, F., Huisman, J., Tognotti, L., Bertei, A., 2022. A comprehensive review and classification of unit operations with assessment of outputs quality in lithium-ion battery recycling. J. Power Sources 546, 231979. https://doi.org/10.1016/j.jpowsour.2022.231979.

Li, J., Wang, G., Xu, Z., 2016. Environmentally-friendly oxygen-free roasting/wet magnetic separation technology for in situ recycling cobalt, lithium carbonate and graphite from spent $LiCoO_2$/graphite lithium batteries. J. Hazard. Mater. 302, 97–104. https://doi.org/10.1016/j.jhazmat.2015.09.050.

Lin, J., Li, L., Fan, E., Liu, C., Zhang, X., Cao, H., Sun, Z., Chen, R., 2020. Conversion mechanisms of selective extraction of lithium from spent lithium-ion batteries by sulfation roasting. ACS Appl. Mater. Interfaces 12 (16), 18482–18489. https://doi.org/10.1021/acsami.0c00420.

Lin, J., Liu, C., Cao, H., Chen, R., Yang, Y., Li, L., Sun, Z., 2019. Environmentally benign process for selective recovery of valuable metals from spent lithium-ion batteries by using conventional sulfation roasting. Green Chem. 21 (21), 5904–5913.

Liu, C., Lin, J., Cao, H., Zhang, Y., Sun, Z., 2019a. Recycling of spent lithium-ion batteries in view of lithium recovery: a critical review. J. Clean. Prod. 228, 801–813.

Liu, P., Xiao, L., Chen, Y., Tang, Y., Wu, J., Chen, H., 2019b. Recovering valuable metals from $LiNi_xCo_yMn_{1-x-y}O_2$ cathode materials of spent lithium ion batteries via a combination of reduction roasting and stepwise leaching. J. Alloy Compd. 783, 743–752. https://doi.org/10.1016/j.jallcom.2018.12.226.

Makuza, B., Tian, Q., Guo, X., Chattopadhyay, K., Yu, D., 2021. Pyrometallurgical options for recycling spent lithium-ion batteries: a comprehensive review. J. Power Sources 491, 229622. https://doi.org/10.1016/j.jpowsour.2021.229622.

Mansur, M.B., Guimarães, A.S., Petraniková, M., 2022. An overview on the recovery of cobalt from end-of-life lithium ion batteries. Miner. Process. Extr. Metall. Rev. 43 (4), 489–509. https://doi.org/10.1080/08827508.2021.1883014.

Mao, J., Li, J., Xu, Z., 2018. Coupling reactions and collapsing model in the roasting process of recycling metals from $LiCoO_2$ batteries. J. Clean. Prod. 205, 923–929. https://doi.org/10.1016/j.jclepro.2018.09.098.

Meng, F., McNeice, J., Zadeh, S.S., Ghahreman, A., 2021. Review of lithium production and recovery from minerals, brines, and lithium-ion batteries. Miner. Process. Extr. Metall. Rev. 42 (2), 123–141. https://doi.org/10.1080/08827508.2019.1668387.

Paoli L. (2022) Electric cars fend off supply challenges to more than double global sales. Accessed 30 January 2022.

Peng, C., Liu, F., Wang, Z., Wilson, B.P., Lundström, M., 2019. Selective extraction of lithium (Li) and preparation of battery grade lithium carbonate (Li_2CO_3) from spent Li-ion batteries in nitrate system. J. Power Sources 415, 179–188. https://doi.org/10.1016/j.jpowsour.2019.01.072.

Ren, G., Xiao, S., Xie, M., Pan, B., Chen, J., Wang, F., Xia, X., 2017. Recovery of valuable metals from spent lithium ion batteries by smelting reduction process based on $FeO–SiO_2–Al_2O_3$ slag system. T. Nonferr. Metal Soc. 27 (2), 450–456. https://doi.org/10.1016/S1003-6326(17)60051-7.

Shahat, A., Hassan, H.M., El-Shahat, M.F., El Shahawy, O., Awual, M.R, 2018. Visual nickel (II) ions treatment in petroleum samples using a mesoporous composite adsorbent. Chem. Eng. J. 334, 957–967. https://doi.org/10.1016/j.cej.2017.10.105.

Shi, J., Peng, C., Chen, M., Li, Y., Eric, H., Klemettinen, L., Lundström, M., Taskinen, P., Jokilaakso, A., 2019. Sulfation roasting mechanism for spent lithium-ion battery metal oxides under SO_2-O_2-Ar atmosphere. JOM 71 (12), 4473–4482. https://doi.org/10.1007/s11837-019-03800-5.

Sloop, S.E., Crandon, L., Allen, M., Koetje, K., Reed, L., Gaines, L., Sirisaksoontorn, W., Lerner, M., 2020. A direct recycling case study from a lithium-ion battery recall. Sustain. Mater. Technol. 25 https://doi.org/10.1016/j.susmat.2020.e00152.

Sloop, S.E., Trevey, J.E., Gaines, L., Lerner, M.M., Xu, W., 2018. Advances in direct recycling of lithium-ion electrode materials. ECS Trans 85, 397–403. https://doi.org/10.1149/08513.0397ECST.

Sun, H., Zhao, K., 2017. Electronic structure and comparative properties of $LiNi_xMn_yCo_zO_2$ cathode materials. J. Phys. Chem. C 121 (11), 6002–6010.

Tang, Y., Xie, H., Zhang, B., Chen, X., Zhao, Z., Qu, J., Xing, P., Yin, H., 2019. Recovery and regeneration of $LiCoO_2$-based spent lithium-ion batteries by a carbothermic reduction vacuum pyrolysis approach: controlling the recovery of CoO or Co. Waste Manag. 97, 140–148. https://doi.org/10.1016/j.wasman.2019.08.004.

Thompson, D.L., Hartley, J.M., Lambert, S.M., Shiref, M., Harper, G.D., Kendrick, E., Anderson, P., Ryder, K.S., Gaines, L., Abbott, A.P., 2020. The importance of design in lithium ion battery recycling–a critical review. Green Chem. 22 (22), 7585–7603.

Träger, T., Friedrich, B., Weyhe, R., 2015. Recovery concept of value metals from automotive lithium-ion batteries. Chem. Ing.-Tech. 87 (11), 1550–1557.

Umicore Group, Umicore - our recycling process, in: https://csm.umicore.com/en/battery-recycling/our-recycling-process/, 2019.

Wentker, M., Greenwood, M., Leker, J., 2019. A bottom-up approach to lithium-ion battery cost modeling with a focus on cathode active materials. Energies 12 (3), 504.

Wesselborg, T., Virolainen, S., Sainio, T., 2021. Recovery of lithium from leach solutions of battery waste using direct solvent extraction with TBP and $FeCl_3$. Hydrometallurgy 202, 105593. https://doi.org/10.1016/j.hydromet.2021.105593.

Xiao, J., Li, J., Xu, Z., 2017. Recycling metals from lithium ion battery by mechanical separation and vacuum metallurgy. J. Hazard. Mater. 338, 124–131. https://doi.org/10.1016/j.jhazmat.2017.05.024.

HSC Chemistry 10. 2022. http://www.hsc-chemistry.net/index.html.

Yun, L., Linh, D., Shui, L., Peng, X., Garg, A., Le, M.L.P., Asghari, S., Sandoval, J., 2018. Metallurgical and mechanical methods for recycling of lithium-ion battery pack for electric vehicles. Resour., Conserv. Recycl. 136, 198–208. https://doi.org/10.1016/j.resconrec.2018.04.025.

Zhang, J., Hu, J., Zhang, W., Chen, Y., Wang, C., 2018a. Efficient and economical recovery of lithium, cobalt, nickel, manganese from cathode scrap of spent lithium-ion batteries. J. Clean. Prod. 204, 437–446. https://doi.org/10.1016/j.jclepro.2018.09.033.

Zhang, X., Li, L., Fan, E., Xue, Q., Bian, Y., Wu, F., Chen, R., 2018b. Toward sustainable and systematic recycling of spent rechargeable batteries. Chem. Soc. Rev. 47 (19), 7239–7302. https://doi.org/10.1039/C8CS00297E.

Zheng, X., Zhu, Z., Lin, X., Zhang, Y., He, Y., Cao, H., Sun, Z., 2018. A mini-review on metal recycling from spent lithium ion batteries. Engineering 4 (3), 361–370.